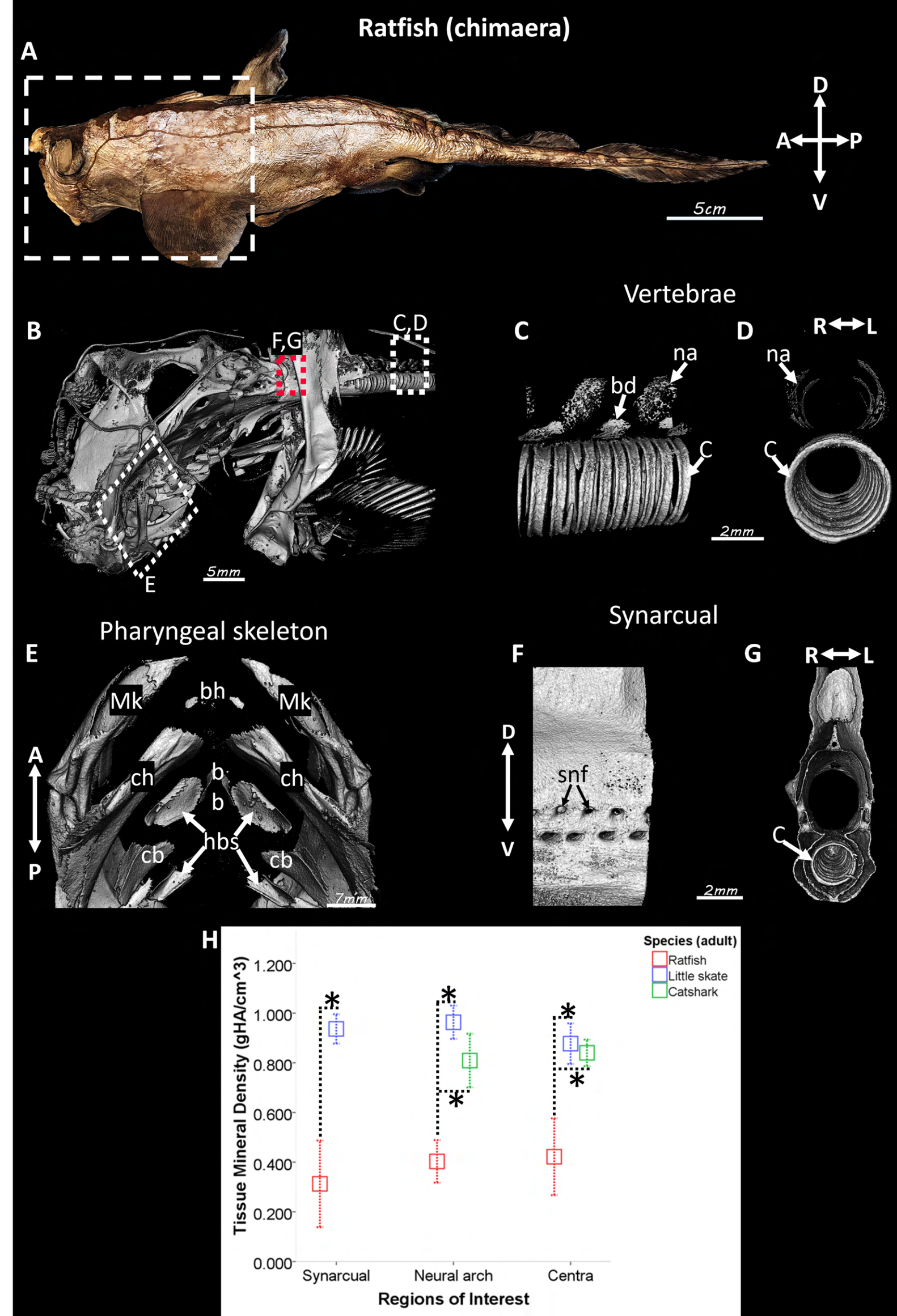
Ratfish (chimaera)
A
D
A
P
V
5cm
Vertebrae
B
F,G
C,D
E
5mm
C
na
bd
C
2mm
D
R
L
na
C
Pharyngeal skeleton
E
Mk
bh
Mk
A
P
ch
b
b
ch
hbs
cb
cb
7mm
Synarcual
F
D
V
snf
2mm
G
R
L
C
H
Species (adult)
Ratfish
Little skate
Catshark
Tissue Mineral Density (gHA/cm^3)
1.200
1.000
0.800
0.600
0.400
0.200
0.000
Synarcual
Neural arch
Centra
Regions of Interest

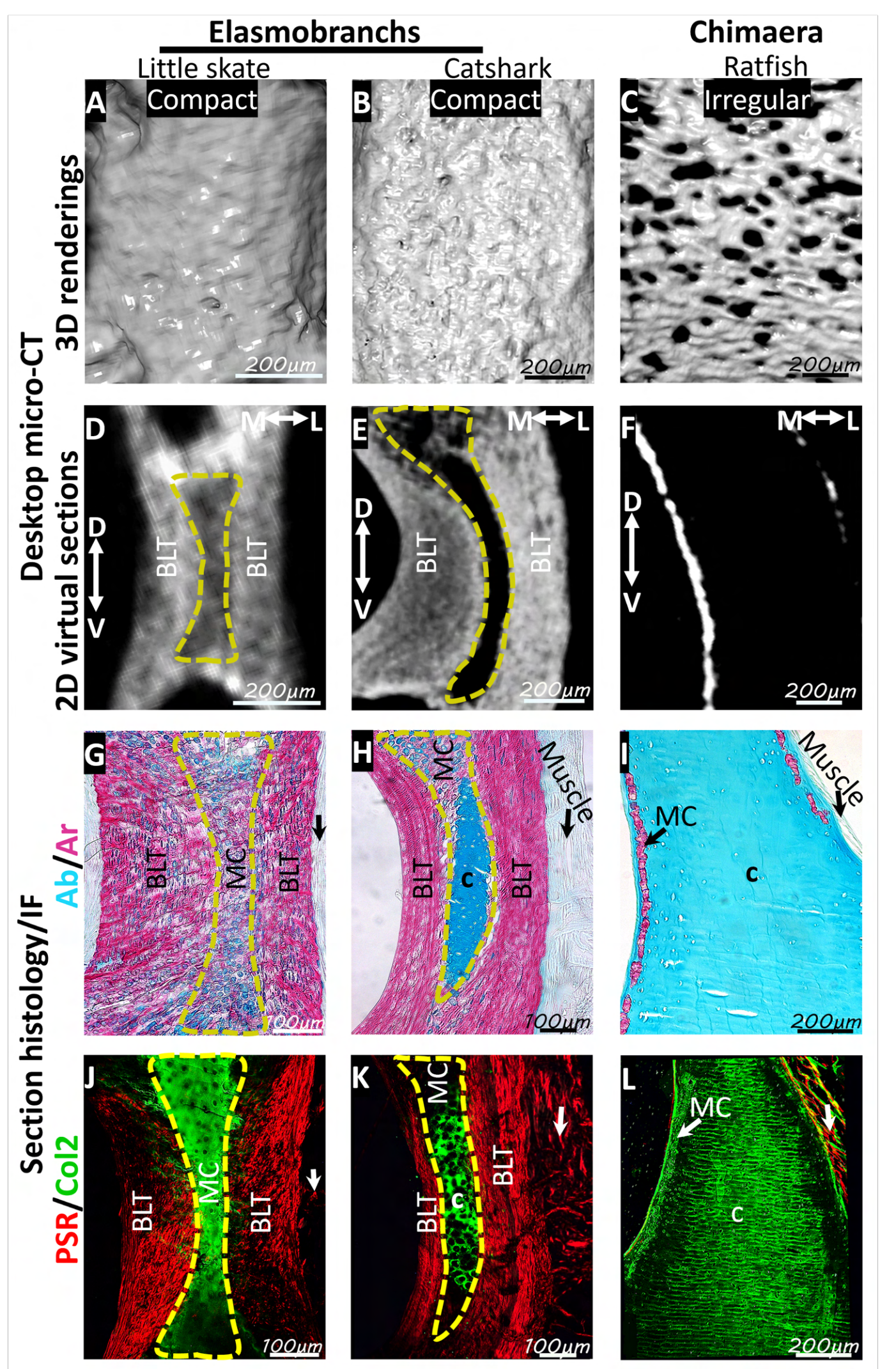
Elasmobranchs
Chimaera
Little skate
Catshark
Ratfish
Compact
Compact
Irregular
Desktop micro-CT
3D renderings
2D virtual sections
Section histology/IF
Ab/Ar
PSR/Col2
A
B
C
D
E
F
G
H
I
J
K
L
200µm
M
L
D
V
BLT
MC
c
Muscle
100µm

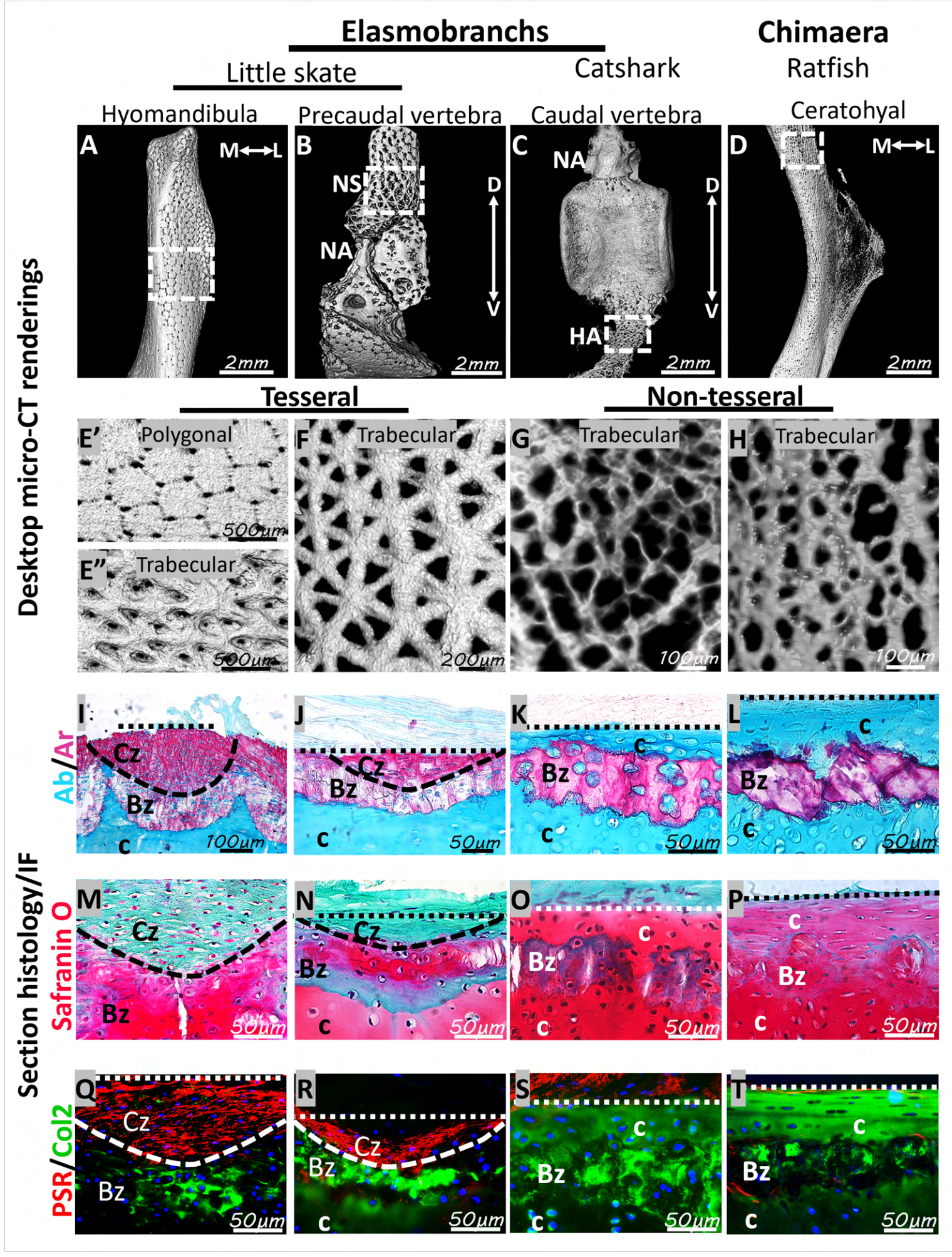
Elasmobranchs
Chimaera
Little skate
Catshark
Ratfish
Hyomandibula
Precaudal vertebra
Caudal vertebra
Ceratohyal
Desktop micro-CT renderings
A
M↔L
2mm
B
NS
NA
D
V
2mm
C
NA
HA
D
V
2mm
D
M↔L
2mm
Tesseral
Non-tesseral
E'
Polygonal
500µm
E"
Trabecular
500µm
F
Trabecular
200µm
G
Trabecular
100µm
H
Trabecular
100µm
Section histology/IF
Ab/Ar
I
Cz
Bz
c
100µm
J
Cz
Bz
c
50µm
K
c
Bz
c
50µm
L
c
Bz
c
50µm
Safranin O
M
Cz
Bz
50µm
N
Cz
Bz
c
50µm
O
c
Bz
c
50µm
P
c
Bz
c
50µm
PSR/Col2
Q
Cz
Bz
50µm
R
Cz
Bz
c
50µm
S
c
Bz
c
50µm
T
c
Bz
c
50µm

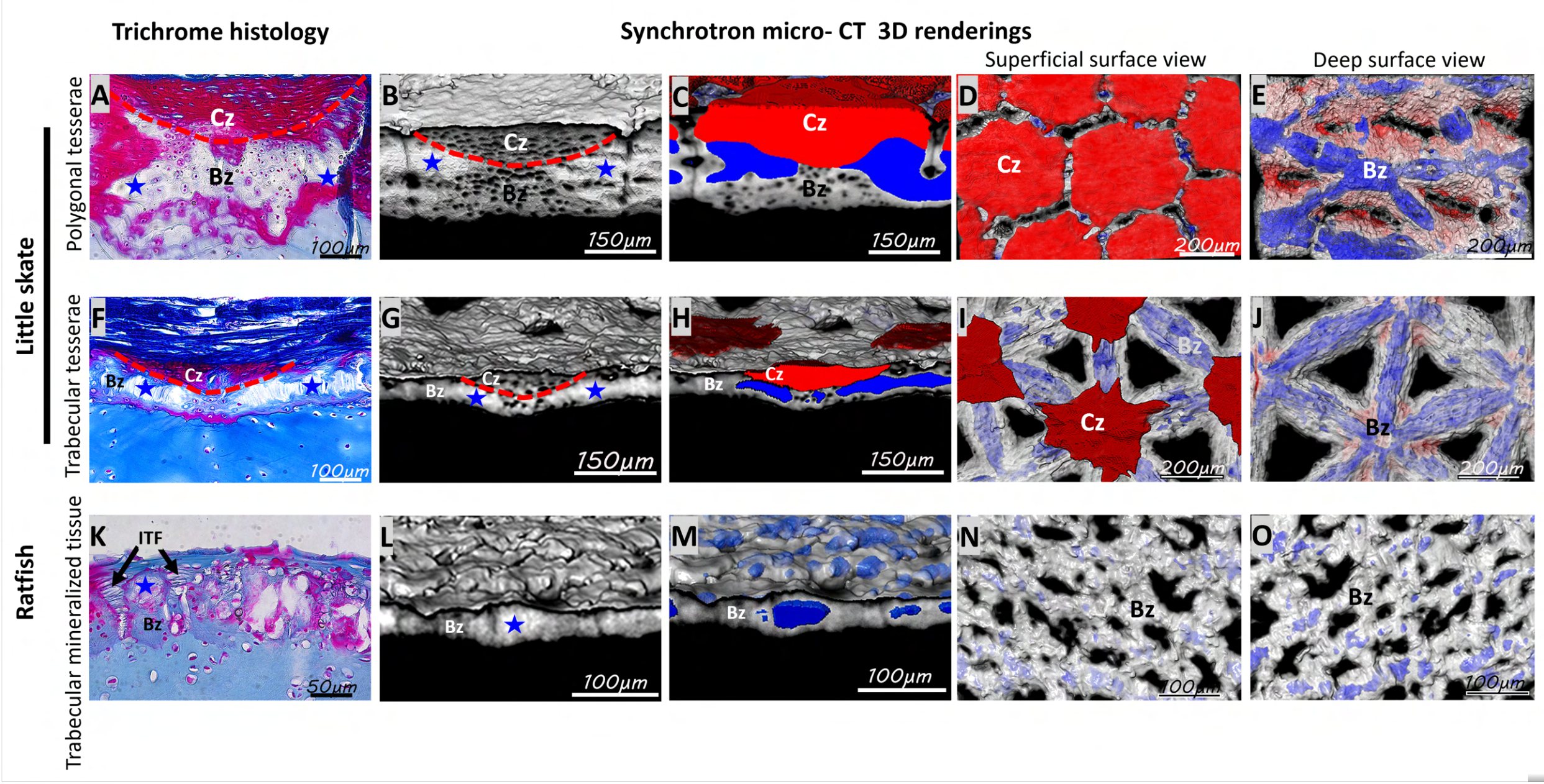
Trichrome histology
Synchrotron micro- CT 3D renderings
Superficial surface view
Deep surface view
Little skate
Ratfish
Polygonal tesserae
Trabecular tesserae
Trabecular mineralized tissue
A
B
C
D
E
F
G
H
I
J
K
L
M
N
O
Cz
Bz
ITF
100µm
150µm
200µm
50µm

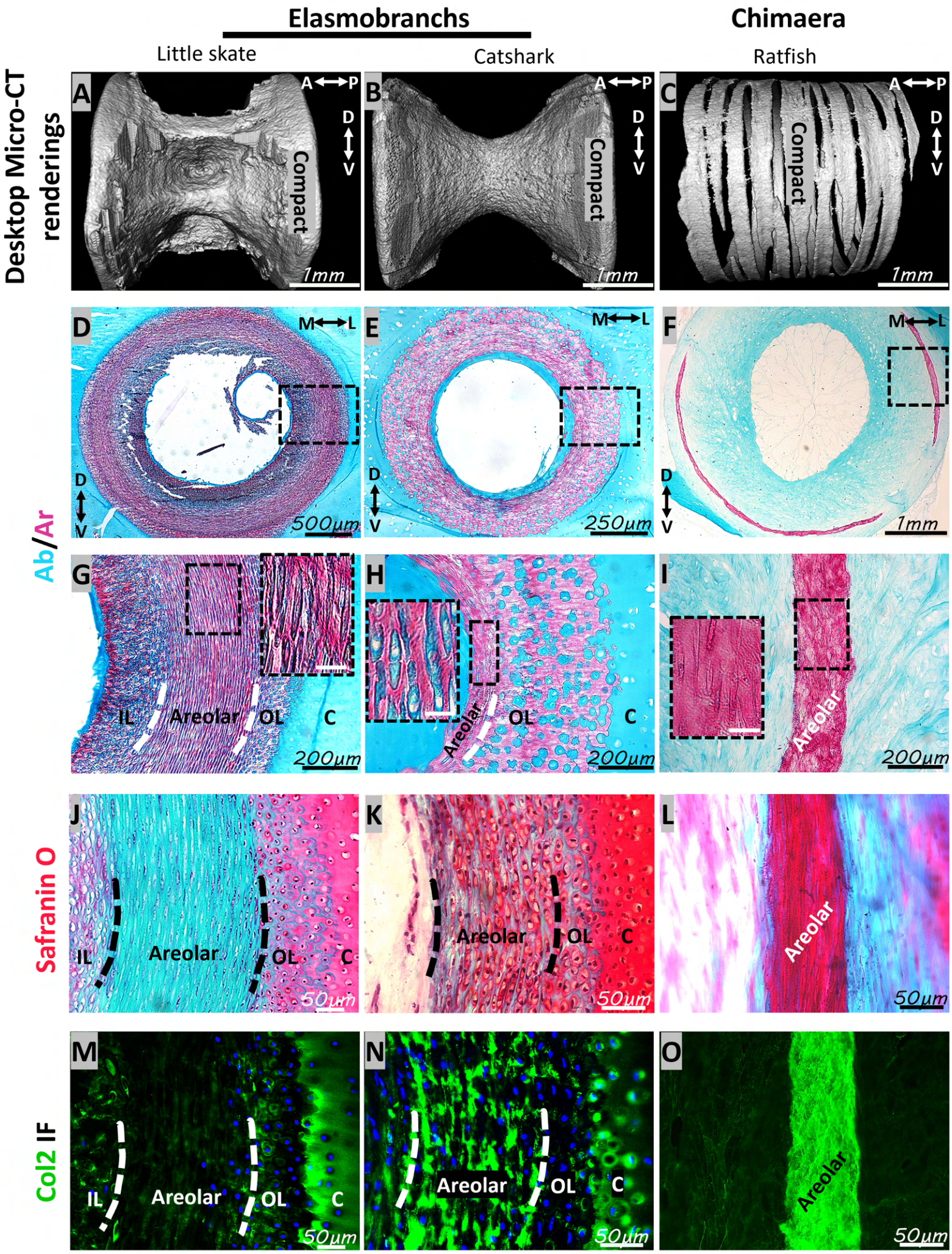
Elasmobranchs
Chimaera
Little skate
Catshark
Ratfish
Desktop Micro-CT renderings
A
B
C
A
P
D
V
Compact
1mm
Ab/Ar
D
E
F
M
L
D
V
500µm
250µm
1mm
G
H
I
IL
Areolar
OL
C
200µm
Safranin O
J
K
L
50µm
Col2 IF
M
N
O

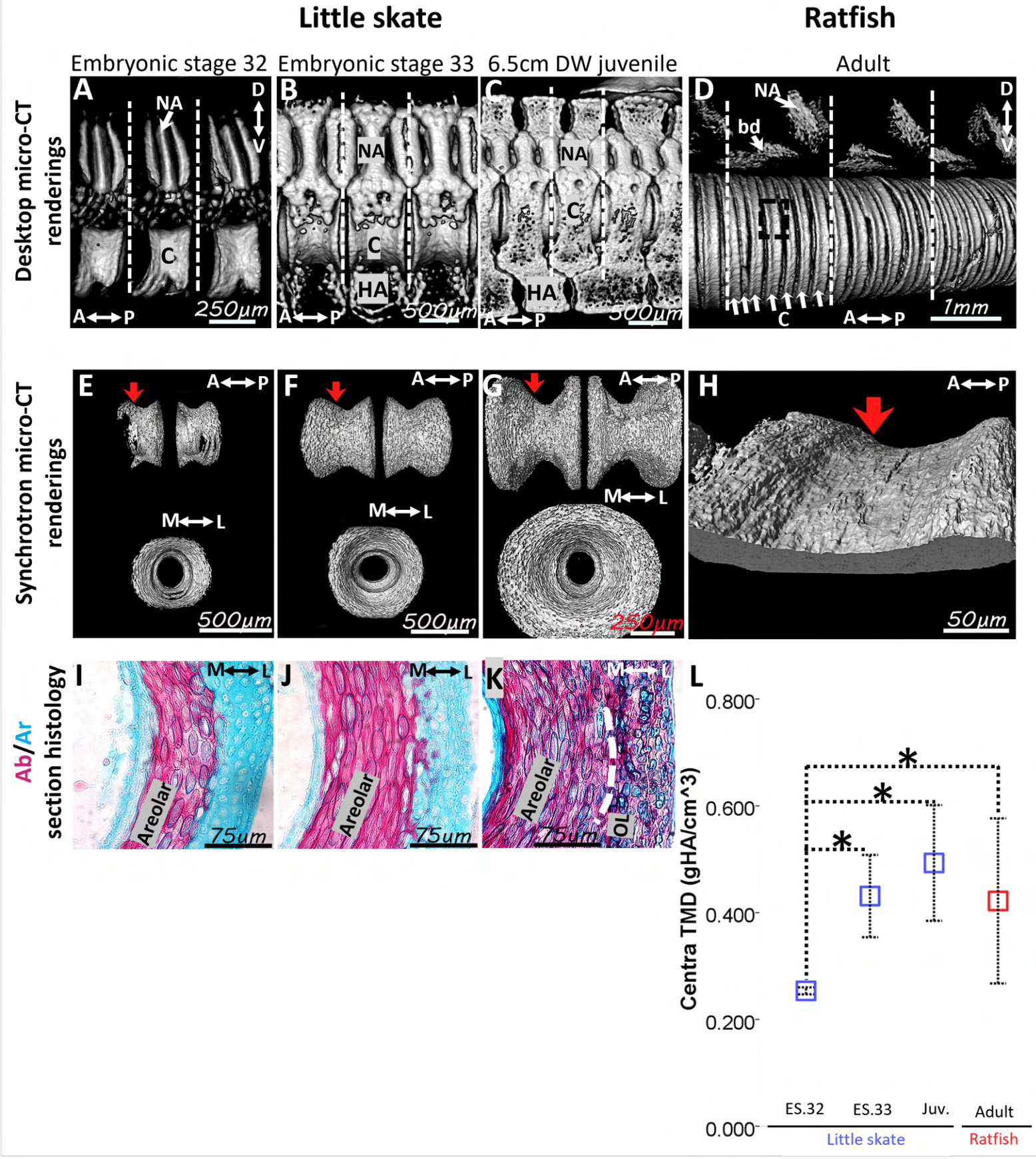
Little skate
Ratfish
Embryonic stage 32
Embryonic stage 33
6.5cm DW juvenile
Adult
Desktop micro-CT renderings
A
NA
D
V
C
A↔P
250µm
B
NA
C
HA
A↔P
500µm
C
NA
C
HA
A↔P
500µm
D
NA
bd
D
V
C
A↔P
1mm
Synchrotron micro-CT renderings
E
A↔P
M↔L
500µm
F
A↔P
M↔L
500µm
G
A↔P
M↔L
250µm
H
A↔P
50µm
Ab/Ar section histology
I
M↔L
Areolar
75um
J
M↔L
Areolar
75um
K
M↔L
Areolar
OL
75um
L
Centra TMD (gHA/cm^3)
0.800
0.600
0.400
0.200
0.000
*
*
*
ES.32
ES.33
Juv.
Adult
Little skate
Ratfish

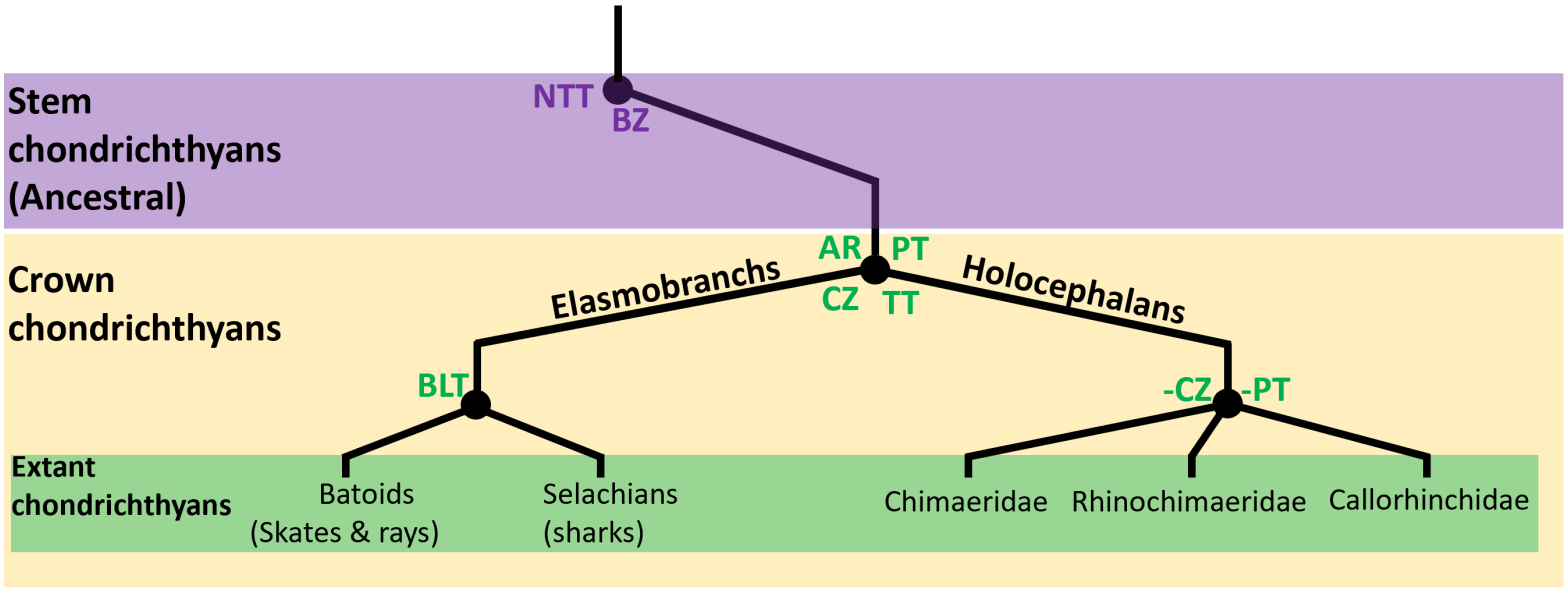

	Batoids (Skates & rays)	Selachians (sharks)	Chimaeridae	Rhinochimaeridae	Callorhinchidae
Neural arch bone-like tissue (BLT)	+	+	-	?	?
Polygonal tesseral mineralization (PT)	+	+/-	-	?	?
Trabecular tesseral mineralization (TT)	+	?	-	?	?
Non-tesseral trabecular mineralization (NTT)	-	+	+	?	?
Tesseral cap zone (CZ)	+/-	+/-	-	?	-
Tesseral or non-tesseral body zone (BZ)	+	+	+	+	+
Areolar Mineralization (AR)	+	+	+	+	-

Derived character

Ancestral character

Extant cartilaginous fishes share trabecular and areolar mineralization patterns, but not tesserae, and evidence for a paedomorphic chimaera skeleton

Oghenevwogaga J. Atake[1], Fidji Berio[2], Melanie Debiais-Thibaud[2], B. Frank Eames[1]

[1]Department of Anatomy, Physiology, and Pharmacology, University of Saskatchewan, Saskatoon, Canada

[2] Institut des Sciences de l'Evolution, University of Montpellier, CNRS, IRD, EPHE, Montpellier, France

Correspondence

B. F. Eames,

Department of Anatomy, Physiology, and Pharmacology, University of Saskatchewan, 2D01-107 Wiggins Rd, Saskatoon, SK, S7N 5E5 Canada

Tel: +1 (306)966-6534

Email: b.frank@usask.ca

Website: https://www.eameslab.ca/

Abstract

A comprehensive study is lacking that clearly defines and directly compares the diverse mineralized endoskeletal tissues exhibited by extant chondrichthyans (elasmobranchs, such as sharks and skates, and holocephalans, such as chimaeras). Tiles of mineralized polygonal structures called tesserae occur at cartilage surfaces in chondrichthyans, but recent studies showing trabecular structures suggest that tesserae are not as common as previously thought. A specific region of tesserae termed cap zone and continuous (not tiled) mineralized elasmobranch neural arches demonstrate bone-like tissues. Areolar mineralized tissue in elasmobranchs is generally considered a unique chondrichthyan feature. Despite these reports, it remains unclear what mineralized endoskeletal features define extant chondrichthyans. To address this question, adult skeletal tissues in two elasmobranchs (little skate and small-spotted catshark) and a chimaera (spotted ratfish) were characterized using synchrotron radiation and desktop micro-CT imaging, and histological and immunofluorescent assays. Data from these extant chondrichthyan representatives suggested that trabecular and areolar mineralization, but not tesserae and bone-like tissues, are shared features of the extant chondrichthyan endoskeleton. Interestingly, three separate analyses argued that the chimaera endoskeleton retains ancestral embryonic features (i.e., paedomorphic). This study further proposes general terminology for character states of the extant chondrichthyan endoskeleton and infers those states in ancestral chondrichthyans.

Key words: chondrichthyan endoskeleton, mineralization patterns, sharks, skates, chimaeras, tesserae, bone-like tissues, paedomorphism

Introduction

The skeleton of chondrichthyans, or cartilaginous fishes, has long fascinated evolutionary biologists (Janvier, 1996; Maisey, 2013; Ørvig, 1951; Smith and Hall, 1990). However, only in the past 15 years has an active research community revealed the histological and molecular complexity of extant chondrichthyan skeletal tissues. Even so, these studies are limited in scope, focussing mostly on specific skeletal features of the Elasmobranchii subclass of extant Chondrichthyes, such as sharks, skates, and rays (Atake et al., 2019; Dean et al., 2017; Eames et al., 2007; Johanson et al., 2012; Kemp and Westrin, 1979; Omelon et al., 2014; Porter et al., 2006; Seidel et al., 2016), with only a couple including the Holocephali subclass, such as chimaera (Gillis et al., 2011; Herbert et al., 2022; Pears et al., 2020; Seidel et al., 2020; Smith et al., 2020). Unfortunately, an in-depth description of the extant holocephalan endoskeleton is severely lacking, leading to a major deficit in understanding skeletal tissue character states across extant chondrichthyans.

Like most vertebrates, skeletal mineralization in extant chondrichthyans occurs by incorporation of biominerals into extracellular compartments of skeletal tissues (Golub, 2009; Lowenstam, 1981; Omelon et al., 2014), giving rise to diverse mineralized tissue types in several anatomical sites of the chondrichthyan endoskeleton. Traditionally recognized as a defining endoskeletal feature of Chondrichthyes, tesserae form a mineralization pattern consisting of an array of distinct, polygonal units at the surface of cartilages (Kemp and Westrin, 1979; Maisey, 2013; Maisey et al., 2021). In skates, however, a recently characterized trabecular mineralization pattern lies directly underneath the polygonal pattern of tesserae (Atake et al.,

2019). In fact, the cartilage surface in several endoskeletal regions of skates and rays only contain the trabecular mineralization pattern (Atake et al., 2019; Jayasankar et al., 2020), suggesting that polygonal tesserae may not be as common as traditionally thought. Like polygonal tesserae, the little skate trabecular mineralization also forms an arrayed pattern, but the repeating units are in the form of trabecular struts interspersed by unmineralized regions, leading us to call them trabecular tesserae (Atake et al., 2019; Atake and Eames, 2021). Descriptions of a trabecular mineralization pattern in the endoskeleton of sharks or chimaeras are currently lacking, leaving open the possibility that this is a phenotype specific to the Batoidea superorder (including skates and rays) of the subclass Elasmobranchii. In some chimaeras, the surfaces of cartilage in the anterior fused vertebrae (synarcual) and chondrocranium have sheets of mineralization that abut one another (Pears et al., 2020; Seidel et al., 2020), but these do not have an arrayed pattern of repeating units, so perhaps they should not be called tesserae.

Recent evidence suggests that histological features of tesserae may vary according to the mineralization pattern. Traditional polygonal tesserae have distinct histological zones, with a cap zone superficial to a body zone near the surface of chondrichthyan cartilage (Atake et al., 2019; Berio et al., 2021; Kemp and Westrin, 1979; Seidel et al., 2016). While skates have polygonal tesserae, trabecular tesserae in little skate have very small or even absent cap zones overlying extensive body zones (Atake et al., 2019). Additionally, specific regions of tesserae termed spokes are hypermineralized and often devoid of cells, and spokes appear to be a common feature of tesserae regardless of their mineralization pattern (Atake et al., 2019; Pears

et al., 2020; Seidel et al., 2020; Seidel et al., 2016). Overall, these data strongly suggest that histological zones of tesserae actually correlate with mineralization patterns.

Some chondrichthyans have mineralized endoskeletal tissues that have been characterized as bone-like (Atake and Eames, 2021). For example, the cap zone of tesserae displays bony features, like elongate cell lacunae in a mineralized ECM of densely packed Col1 fibers (Atake et al., 2019; Kemp and Westrin, 1979; Seidel et al., 2017; Seidel et al., 2016). Unlike the cap zone, the body zone displays typical features of hyaline cartilage, which is the main cartilage type in vertebrates (Goldring et al., 2006). The body zone consists of round chondrocyte lacunae embedded in a mineralized matrix abundant in loosely packed type II collagen (Col2) fibers and sulfated glycosaminoglycans (Enault et al., 2015; Seidel et al., 2017). As another example of bone-like tissue, many elasmobranch species have a non-tiled, mineralized perichondral tissue in their neural arches (Atake et al., 2019; Berio et al., 2021; Bordat, 1987; Eames et al., 2007; Kemp and Westrin, 1979; Seidel et al., 2016). The neural arch bone-like tissue demonstrates morphological and histological features of perichondral bone, including a compact mineralization pattern, elongate cell lacunae, canaliculi-like channels connecting adjacent lacunae, and tightly packed type I collagen (Col1) fibers (Bordat, 1987; Eames et al., 2007; Kemp and Westrin, 1979; Peignoux-Deville et al., 1982; Rossert and de Crombrugghe, 2002; Seidel et al., 2017). Bone-like tissues might be a defining feature of extant chondrichthyans, but relevant data from chimaeras are needed.

Finally, areolar mineralized tissue is generally considered a unique feature of the extant chondrichthyan endoskeleton, characterized mostly in elasmobranchs as large sheets of mineralization in the notochordal sheath of the vertebral body (centrum) (Didier, 1995;

106 Ridewood and MacBride, 1921). Areolar mineralized tissue typically contains concentric
107 lamellae of elongate lacunae in a fibrocartilage-like extracellular matrix and a compact
108 mineralization pattern (Atake et al., 2019; Criswell et al., 2017; Dean and Summers, 2006;
109 Eames et al., 2007). Mineralized centra are not thought to be common in chimaeras, but when
110 present, they can appear as multiple mineralized rings in each vertebral segment, which
111 contrasts with the grossly biconcave morphology of segmented centra in elasmobranchs
112 (Gadow and Abbott, 1895).

113 With hopes of revealing shared and clade-specific features among chondrichthyans,
114 here we clarify many of the unresolved issues highlighted above. Testing the hypothesis that
115 extant chondrichthyans share histological and morphological features of endoskeletal
116 mineralized tissues, adult tissues in several endoskeletal regions of the small-spotted catshark
117 *Scyliorhinus canicula* (shark), little skate *Leucoraja erinacea* (skate), and spotted ratfish
118 *Hydrolagus colliei* (chimaera) were characterized using synchrotron radiation and desktop
119 micro-CT imaging, and histological and immunofluorescent assays. The data argue that
120 trabecular and areolar, but not polygonal, mineralization patterns are shared by extant
121 chondrichthyans. For ratfish, tesseral mineralization, cap zones, and neural arch bone-like
122 tissues were absent, and three separate analyses argued that this chimaera displays skeletal
123 paedomorphosis, or retention of ancestral embryonic features (Garstang, 1922). While
124 additional chondrichthyan representatives can bolster these findings, this study proposes
125 general terminology for character states of the extant chondrichthyan endoskeleton,
126 concluding that ancestral chondrichthyans had trabecular and areolar mineralization patterns,
127 with tesserae likely lost in various extant chondrichthyan clades.

128

129 ## Results

130 **Adult mineralized tissues in spotted ratfish had lower tissue mineral density (TMD) than little**
131 **skate or small-spotted catshark**

132 To assess whether chimaeras demonstrate skeletal mineralization in anatomical sites that
133 are homologous to those of elasmobranchs, 3D rendering of micro-CT images of anterior
134 regions of adult ratfish were qualitatively and quantitatively analyzed (Fig. 1A,B). Micro-CT
135 images revealed mineralized tissues in several endoskeletal regions including segmented
136 vertebral neural arches and centra (Fig. 1C,D), several skeletal elements in the pharyngeal
137 skeleton (Fig. 1E), and the fused vertebral synarcual (Fig. 1F,G). Although elasmobranchs
138 mineralize neural arches in their precaudal and caudal vertebrae (Atake et al., 2019; Berio et al.,
139 2021; Eames et al., 2007), mineralized neural arches were present mainly in precaudal
140 vertebrae of ratfish (Fig. 1C,D; data not shown). Mineralized skeletal elements in the
141 pharyngeal skeleton included the basihyal, Meckel's, ceratohyal, basibranchial, hypobranchials,
142 and ceratobranchial (Fig. 1E). Spinal nerve foramina are common in the synarcual of
143 cartilaginous fishes and were present in the ventral sides of the ratfish synarcual (Fig. 1F;
144 Claeson, 2011; Johanson et al., 2015; Pears et al., 2020). Unlike the synarcual in skates and
145 other batoids, where distinct vertebral parts are not discernible (Atake et al., 2019; Claeson,
146 2011), the synarcual in ratfish had distinct mineralized centra (Fig. 1G).

147 TMDs of the synarcual, neural arches, and centra in ratfish, little skate, and catshark were
148 quantitated and compared, where possible, since sharks do not have a synarcual (Fig. 1H). To
149 make TMD analysis of the synarcual in ratfish and little skate more comparable, distinct centra

150 in the ratfish synarcual were segmented and excluded. The average TMD of the ratfish
151 synarcual was 0.31± 0.11 gHA/cm^3, significantly lower than the TMD of the little skate
152 synarcual, which was 0.94 ± 0.04 gHA/cm^3 (Fig. 1H; p= 6.5x10^{-4}). Similarly, the TMD of ratfish
153 neural arches (0.40 ± 0.05 gHA/cm^3) was significantly lower than the TMD of neural arches of
154 either little skate (0.96 ± 0.04 gHA/cm^3; p=4.5x10^{-7}) or catshark (0.81 ± 0.04 gHA/cm^3; p=9 x10^{-6})
155 (Fig. 1H). The average TMD of ratfish centra (0.42 ± 0.10 gHA/cm^3) was also significantly lower
156 than the TMD of centra of either little skate (0.88 ± 0.05 gHA/cm^3; p=3.4 x10^{-5}) or catshark (0.84
157 ± 0.02 gHA/cm^3; p=1.1 x10^{-4}) (Fig. 1H). TMD of segmented centra within the ratfish synarcual
158 was similar to that of centra in segmented vertebrae of ratfish (0.46 ± 0.11 gHA/cm^3). These
159 analyses showed that the synarcual, neural arches, and centra in ratfish had significantly lower
160 TMDs compared to homologous elements in little skate and catshark.
161
162 **Neural arches in ratfish lacked bone-like tissue**
163 To clarify whether chimaeras have bone-like tissue like elasmobranchs, micro-CT and
164 histological analyses of neural arches in segmented precaudal vertebrae of ratfish were
165 compared to neural arches in segmented precaudal vertebrae of little skate and catshark.
166 Unlike the compact mineralization pattern displayed by neural arch bone-like tissue in little
167 skate and catshark (Fig. 2A,B; Atake et al., 2019; Berio et al., 2021), mineralization of neural
168 arches in ratfish was organized in an irregular pattern of small compact and trabecular regions
169 (Fig. 2C). Neural arch bone-like tissues in little skate and catshark were extensively mineralized
170 and surrounded a cartilaginous core (Fig. 2D,E,G,H). By contrast, mineralized tissues in ratfish
171 were restricted to the medial and lateral periphery of the cartilaginous neural arches (Fig. 2F,I).

172 Histologically, mineralization of continuous, bone-like tissues in neural arches of little
173 skate and catshark was marked by Alizarin red (Fig. 2G,H). Alizarin red staining also marked
174 mineralized tissues in ratfish neural arches, but they were much thinner and not continuous
175 (Fig. 2I). Stained with both Alizarin red and Alcian blue, the neural arch core in little skate was
176 mineralized cartilage, while that of the catshark was mostly unmineralized cartilage (Fig. 2G,H).
177 Alcian blue staining also showed that most of the neural arches in ratfish was unmineralized
178 cartilage (Fig. 2I). Birefringence of tissue fibers was enhanced using picrosirius red staining and
179 observed under polarized light (Eames et al., 2007). Birefringent fibers (likely reticular) were
180 observed in muscles lateral to neural arches in all three species (Fig. 2J-L). Birefringence of
181 tightly packed collagen fibers in neural arch bone-like tissues was observed in little skate and
182 catshark (Fig. 2J,K), but no birefringence was observed in ratfish neural arches (Fig. 2L). Only the
183 cartilaginous core in neural arches of little skate and catshark demonstrated Col2
184 immunofluorescence (Fig. 2J,K), whereas most regions (including unmineralized cartilage and
185 mineralized tissue) in ratfish neural arches demonstrated Col2 immunofluorescence (Fig. 2L).
186 These results showed that bone-like tissue was absent in neural arches of ratfish, and the
187 irregular pattern of mineralized tissue in ratfish neural arches was mineralized cartilage.
188

189 **Trabecular mineralization was present in little skate, catshark, and ratfish**

190 To clarify whether polygonal or trabecular tesserae are defining endoskeletal features of
191 extant chondrichthyans, morphological patterns and histological features of mineralized tissues
192 were characterized in several endoskeletal regions, including hyomandibulae and precaudal
193 vertebrae of little skate, caudal vertebrae of catshark, and ceratohyals of ratfish (Fig. 3A-D).

Similar to many other skeletal elements in elasmobranchs (Atake et al., 2019; Kemp and Westrin, 1979; Maisey, 2013; Marrama et al., 2019; Seidel et al., 2016; Wilga and Ferry, 2015), desktop micro-CT renderings of hyomandibulae in little skate showed polygonal tesserae, displaying a superficial, arrayed pattern of repeating polygonal units (Fig. 3A,E'; Atake et al., 2019; Kemp and Westrin, 1979; Maisey, 2013; Marrama et al., 2019; Seidel et al., 2016; Wilga and Ferry, 2015). In little skate, an arrayed pattern of repeating trabecular units was located underneath the superficial polygonal tesseral pattern (Fig. 3E"; Atake et al., 2019). In multiple regions examined in catshark (vertebrae and ceratohyals) and ratfish (vertebrae, pharyngeal skeleton, and the synarcual), a polygonal mineralization pattern was not observed. Non-tesseral mineralization patterns were observed in some regions of the catshark and ratfish. For example, mineralized tissues in catshark haemal arches and ratfish ceratohyals had a trabecular pattern, like that of trabecular tesserae in the vertebral neural spine of little skate, but the trabecular pattern in catshark and ratfish was not as clearly organized into arrays of repeating trabecular units (Fig. 3F-H).

To assess whether trabecular mineralization in catshark and ratfish was histologically similar to trabecular mineralization of tesserae in little skate, features of histological cross sections were compared to tesserae in little skate. Like polygonal and trabecular tesserae in little skate, Alcian blue and Alizarin red staining showed mineralized tissues in discrete perichondral regions of catshark haemal arches and ratfish ceratohyals (Fig. 3I-L; perichondrium marked by straight dashed line). In little skate, a bone-like cap zone was just below the perichondrium, stained more intensely than the body zone with Alizarin red, and was present in both polygonal and trabecular tesserae (Fig. 3I,J). In catshark and ratfish, bone-like cap zones

216 were absent, and an unmineralized, Alcian blue-positive cartilage separated Alizarin red-
217 positive mineralized tissues from overlying perichondrium (Fig. 3K,L). Matrix of the little skate
218 bone-like cap zone was fast green-positive and had birefringent collagen fibers, but these
219 staining patterns were not observed in catshark and ratfish (Fig. 3M-T). Instead, regions just
220 below the perichondrium of catshark haemal arches and ratfish ceratohyals were Safranin O-
221 positive and Col2-positive cartilage (Fig. 3O,P,S,T). Staining patterns near the cartilage surface
222 of catshark and ratfish were consistent with those of mineralized cartilage in the tesseral body
223 zone of the little skate, although chondrocyte lacunae in these regions were not obvious in
224 ratfish (Fig. 3I-T). Therefore, histological features of trabecular mineralized tissues in catshark
225 haemal arches and ratfish ceratohyals were similar to only the body zones of tesserae in the
226 little skate, which consisted of mineralized cartilage.
227

228 **Cap zones correlated with polygonal tesseral mineralization patterns, while body zones**
229 **correlated with trabecular mineralization patterns**

230 Given that trabecular tesserae typically have small or even absent cap zones, and
231 polygonal tesserae typically have large cap zones, histology and micro-CT segmentation were
232 used to see whether tesseral histological features correlated with tesseral mineralization
233 patterns. In little skate, the larger and smaller cap zones in polygonal and trabecular tesserae,
234 respectively, were similarly marked by Trichrome's acid fuchsin and elongated lacunae (Fig.
235 4A,F). Spokes were located below the cap zone, distinguished on histological sections by the
236 facts that they often appeared as tears or sectioning artifacts when demineralized, and they did
237 not stain strongly with any Trichrome dye (Fig. 4A,F). Non-spoke regions of the body zone

238 stained either slightly blue with Trichrome's aniline blue or magenta with Trichrome's acid
239 fucshin.

240 Enough histological features of tesserae were also visible in synchrotron radiation
241 micro-CT renderings, making it possible to segment and analyze the spatial correlation between
242 tesseral mineralization patterns and histological features (Fig. 4A-J). Segmentation of 3D
243 renderings of polygonal tesserae showed clearly that the cap zones were responsible for the
244 superficial polygonal mineralization pattern (red in Fig. 4B-D). Hypermineralized spokes were
245 restricted to the body zone, and their segmentation from 3D renderings demonstrated that
246 they were responsible for the deeper trabecular mineralization pattern of polygonal tesserae
247 (blue in Fig. 4B,C,E). Unlike polygonal tesserae, trabecular tesserae in little skate displayed
248 identical trabecular mineralization patterns whether viewed from the superficial or deep
249 surfaces of the cartilage (Fig. 4I,J). The smaller cap zones in trabecular tesserae were discernible
250 on the superficial surface, but they were not as laterally extensive as cap zones of polygonal
251 tesserae (Fig. 4C,D,H,I). Thus, larger and laterally extensive cap zones appeared to be the
252 reason why polygonal tesserae displayed a superficial polygonal mineralization pattern.
253 Trabecular mineralization patterns in both polygonal and trabecular tesserae appeared to
254 derive mostly from spokes, but also from non-spoke regions, within body zones.

255 A cap zone was absent in ratfish, but Trichrome staining patterns and other histological
256 features of the body zone and spokes were similar to tesserae in little skate, so correlations
257 between spokes and trabecular mineralization patterns were also analyzed (Fig. 4K-O). Some
258 histological features of tesserae, such as body zones, spokes, and intertesseral fibers, were
259 apparent in the trabecular mineralization pattern of the ratfish ceratohyal (Fig. 2H; Fig. 4K;

Seidel et al., 2020). Like trabecular tesserae in little skate, the superficial and deep surfaces of the trabecular mineralization in ratfish were identical (Fig. 4I,J,N,O). However, segmentation of 3D renderings showed that spokes in ratfish were patchy and did not display the arrayed pattern seen in trabecular tesserae of little skate (Fig. 4A-O). Therefore, compared to little skate, the less-organized spokes in body zones of ratfish correlated with the non-tesseral trabecular mineralization pattern.

Ratfish centra contained areolar mineralized tissue

Some chimaeras were reported to mineralize their centra like elasmobranchs, but areolar mineralized tissue has never been carefully characterized in chimaeras (Didier, 1995; Gadow and Abbott, 1895; Ridewood and MacBride, 1921). To clarify whether chimaeras have areolar mineralized tissue, morphological and histological features of ratfish centra were compared to those of little skate and catshark, two elasmobranch species who are recognized to have areolar mineralization (Atake et al., 2019; Clement, 1992; Criswell et al., 2017). Like elasmobranchs, each centrum in ratfish precaudal vertebrae demonstrated a compact mineralization pattern (Fig. 5A-C). However, precaudal vertebrae in ratfish had multiple rings of centra per vertebral segment (i.e., unit with paired neural arches and basidorsals), and no ratfish centrum displayed the typical biconcave gross morphology associated with elasmobranch centra (Fig. 5A-C).

Alizarin red section histology showed that centra in little skate, catshark, and ratfish comprised of rings of mineralized tissue spanning different numbers of centrum layers (Fig. 5D-I). Areolar mineralized tissues in the middle layer of the centrum of little skate, catshark, and

282 ratfish had elongate cell lacunae organized in concentric lamellae (inserts in Fig. 5G-I; Atake et
283 al., 2019; Criswell et al., 2017; Eames et al., 2007), and they were birefringent (data not shown).
284 In addition to areolar mineralized tissue in the middle layer of the centrum, inner and outer
285 layers of the little skate centrum contained mineralized cartilage (Fig. 5G,J,M), while the outer
286 layer of the catshark centrum had mineralized cartilage (Fig. 5H,K,N). Markers of cartilage
287 differed in areolar mineralized tissue among little skate, catshark, and ratfish. In little skate,
288 areolar mineralized tissue did not display Safranin O staining or Col2 immunofluorescence (Fig.
289 5J,M). In catshark, areolar mineralized tissue demonstrated weak Safranin O staining and Col2
290 immunofluorescence (Fig. 5K,N). By contrast, areolar mineralized tissue in ratfish had relatively
291 strong Safranin O staining and Col2 immunofluorescence (Fig. 5L,O). Overall, these data
292 suggested that ratfish have areolar mineralized tissue, which had been previously characterized
293 mostly in elasmobranchs (Criswell et al., 2017; Eames et al., 2007; Ridewood and MacBride,
294 1921).
295
296 **Embryological analyses of little skate centra suggested that adult ratfish had paedomorphic**
297 **centra**
298 To shed light on differences in morphology between adult elasmobranch and ratfish
299 centra (Fig. 5A-C), morphological and histological features of centra in a developmental series
300 of little skate were compared to those of adult ratfish. Centra in elasmobranchs are thought to
301 acquire a biconcave morphology during development when the perichordal sheath becomes
302 constricted by mesenchymal cells (Gadow and Abbott, 1895). In little skate embryos and
303 juveniles, desktop micro-CT renderings showed mineralization in the centrum and pairs of

304 neural arches, basidorsals, and haemal arches of each vertebral segment (Fig. 6A-C). Expanding
305 upon recent work showing that anterior and posterior segments of somites fuse during skate
306 vertebral development, similar to tetrapods (Criswell and Gillis, 2020), independent anterior
307 and posterior mineralizations of each interneural appeared to later fuse during development. In
308 ratfish, each vertebral segment of paired neural arches and basidorsals had an average of six
309 centra (Fig. 6D). Synchrotron radiation (SR) micro-CT renderings showed that centra in little
310 skate stage 32 embryos were slightly constricted in the middle of each element's anterior-
311 posterior axis, and this constriction progressed through 6.5 cm disc width juveniles, when the
312 classic biconcave morphology became obvious (Fig. 6E-G). SR micro-CT renderings showed that
313 adult ratfish centra were constricted to a similar extent as centra in little skate embryos (Fig.
314 6E,F,H). In little skate embryos, Alcian blue and Alizarin red section histology showed that the
315 areolar mineralized tissue initiated in the middle layer of the centrum and had elongate cell
316 lacunae organized in concentric lamellae, similar to that observed in adult ratfish (Fig. 5F; Fig.
317 6I,J). At later developmental stages of little skate, such as 6.5 cm DW juveniles, the outer layer
318 of the centrum also demonstrated mineralized cartilage (Fig. 6K). These morphological and
319 histological similarities of centra in little skate embryos and adult ratfish suggested that adult
320 ratfish retained an embryonic form of centra, a phenomenon termed paedomorphism
321 (Garstang, 1922).

322 To further test the possibility that ratfish had paedomorphic centra, TMDs of centra in
323 the developmental series of little skate were compared to that of adult ratfish, because TMD of
324 skeletal elements tends to increase during development (Fig. 1H; Forbes, 1976). TMD of little
325 skate centra increased significantly from stage 32 to stage 33 embryos (p= 9.5 x10^{-3}), while TMD

326 of 6.5 cm DW juveniles was only significantly higher than TMD of stage 32 embryos (Fig. 6L;
327 p=9.6 x10^{-4}). TMD of adult ratfish centra was significantly higher than TMD of centra in little
328 skate stage 32 embryos, but it was statistically indistinguishable from TMD of centra in little
329 skate stage 33 embryos and 6.5 cm DW juveniles (Fig. 6L). In addition to morphological
330 similarities, similar TMDs of centra from little skate embryos and adult ratfish argued strongly
331 that ratfish had paedomorphic centra.
332

333 **Discussion**

334 Which tissues are common in the extant chondrichthyan endoskeleton? Bone-like and
335 areolar tissues have been characterized in several members of the chondrichthyan subclass
336 Elasmobranchii, such as sharks, skates, and rays, (Atake et al., 2019; Berio et al., 2021; Bordat,
337 1987; Kemp and Westrin, 1979; Ørvig, 1951; Peignoux-Deville et al., 1982; Seidel et al., 2016). In
338 addition, polygonal tesserae are traditionally associated with chondrichthyans (Atake et al.,
339 2019; Kemp and Westrin, 1979; Maisey, 2013; Marrama et al., 2019; Seidel et al., 2016; Wilga
340 and Ferry, 2015), but trabecular tesserae were recently characterized in skates and rays (Atake
341 et al., 2019; Jayasankar et al., 2020).

342 Two main qualities of this paper go a long way in revealing features of the ancestral
343 chondrichthyan endoskeleton. First, we clearly identifed discrete character states of the extant
344 chondrichthyan endoskeleton (Fig. 7), helping to unify terminology of important features for
345 the growing chondrichthyan research community. Second, we presented extensive, side-by-side
346 comparative data across selected representatives of extant chondrichthyans, two
347 elasmobranch species (little skate and small-spotted catshark) and one chimaera (spotted

348 ratfish). The inclusion of a representative of chimaeras is another critical aspect of this paper,
349 because the other chondrichthyan subclass Holocephali is a severely understudied clade that
350 must be considered when inferring ancestral chondrichthyan traits.

351 Our data provided a critical comparison of character states of the extant chondrichthyan
352 endoskeleton across various species (Fig. 7), especially since previous characterization of
353 skeletal mineralization in other adult chimaeridaes neither focused on segmented neural arches
354 nor clarified histological zones of tesserae (Berio et al., 2021; Debiais-Thibaud, 2018; Pears et
355 al., 2020; Seidel et al., 2020). Morphological and histological features of bone-like tissues in
356 neural arches or tesseral cap zones were present in little skate and catshark, but absent in
357 ratfish. While these data refute the hypothesis that bone-like tissues generally are a
358 symplesiomorphic (shared ancestral) feature of extant chondrichthyans, they further support
359 the hypothesis that neural arch perichondral bone-like tissue is a synapomorphic (shared
360 derived) character of elasmobranchs (Fig.7; Atake et al., 2019; Berio et al., 2021; Maisey et al.,
361 2021). On the other hand, similar histological features of centra were observed in little skate,
362 catshark, and ratfish, and histological features of multiple-ringed centra in other chimaera
363 should be determined (Fig. 5D-I; Fig. 7; Didier, 1995). Since stem chondrichthyans did not
364 typically mineralize their centra, areolar mineralized tissue is likely a synapomorphic character
365 of crown chondrichthyans (Fig. 7; Maisey et al., 2021; Miles, 1970).

366 In what appears to be a newly-defined symplesiomorphy of crown chondrichthyans,
367 trabecular mineralization occurs in many endoskeletal regions in several elasmobranch and
368 chimaera species, including some fossil chondrichthyans (Fig. 3; Fig. 7; Atake et al., 2019;
369 Coates et al., 2018; Frey et al., 2019; Jayasankar et al., 2020; Maisey et al., 2021). While

370 trabecular mineralization always occurred near the surface of cartilage, the exact mineralization
371 pattern varied among extant chondrichthyans. Little skate had arrayed patterns of discrete
372 trabecular units, similar to the repeating polygonal units of traditional tesserae, supporting
373 their description as trabecular tesserae (Fig. 7). On the other hand, trabecular mineralization in
374 catshark and ratfish did not show arrayed patterns of discrete units. While this non-arrayed
375 trabecular mineralization pattern had not been characterized before in extant chondrichthyans,
376 it is also evident in recent images published from the chimaeras *Callorhinchus milii* and
377 *Chimaera monstrosa* (Pears et al., 2020; Seidel et al., 2020). To distinguish this pattern from the
378 regular, arrayed patterns of polygonal and trabecular tesserae, we propose the term "non-
379 tesseral trabecular mineralization" as a new plesiomorphic (ancestral) character of
380 chondrichthyans (Fig. 7; Maisey et al., 2021). Interestingly, some fossil chondrichthyans also
381 appear to display non-tesseral trabecular mineralization in their endoskeletons (Coates et al.,
382 2018; Frey et al., 2019; Ørvig, 1951).

383 Cap and body zones are histological terms that traditionally describe chondrichthyan
384 tesserae (Dean and Summers, 2006; Kemp and Westrin, 1979), but data from adult samples of
385 little skate, catshark, and ratfish argued that the body zone is the only histological zone of
386 endoskeletal mineralization shared by extant chondrichthyans. Published histological data of
387 tesserae are few and limited to sharks, skates, and rays, where cap and body zones have been
388 reported (Atake et al., 2019; Berio et al., 2021; Eames et al., 2007; Enault et al., 2015; Kemp and
389 Westrin, 1979; Pears et al., 2020; Seidel et al., 2017). While Fast green staining and birefringent
390 fibers marked the cap zones in both polygonal and trabecular tesserae in little skate, non-
391 tesseral trabeculae in catshark and ratfish did not have discernible cap zones. In contrast to

392 commonly-accepted knowledge, these catshark data suggest that even sharks do not always
393 have the cap zone. Taken alongside recent published data (Maisey et al., 2021; Pears et al.,
394 2020; Seidel et al., 2020), no living species of chimaera likely has cap zones. On the other hand,
395 Safranin O staining and Col2 immunofluorescence showed that histological body zones
396 generated the mineralized endoskeletal cartilage of little skate, catshark, and ratfish. In total,
397 these data suggest that the ancestral stem chondrichthyan generated most of its endoskeletal
398 mineralization with histological body zones, although as the next paragraph highlights, cap
399 zones might have been lost secondarily in chimaera and some shark species (Fig. 7).

400 Digitally segmented 3D regions of micro-CT renderings showed, for the first time, exact
401 spatial correlations between histological zones and mineralization patterns, potentially
402 impacting histological interpretations of fossils. Strikingly, large and laterally extensive cap
403 zones were the basis of the traditional polygonal tesseral mineralization pattern in little skate.
404 Accordingly, similar polygonal tesserae recently described in fossil holocephalans likely have
405 cap zones in addition to body zones and a trabecular tesseral mineralization underlying the
406 polygonal mineralization pattern, and these might have been lost secondarily during
407 holocephalan evolution (Fig. 3E; Fig. 4; Fig. 7; Atake et al., 2019; Pears et al., 2020). Careful
408 description of polygonal tesserae in fossil elasmobranchs and holocephalans can clarify this
409 point. Two other correlations were identified here in body zones. First, spokes were located in
410 body zones. Second, spoke and non-spoke regions of the body zone underlie the trabecular
411 mineralization patterns, regardless of whether these were organized as arrayed tesserae or not.
412 Spokes appeared much more spatially organized in polygonal tesserae and trabecular tesserae
413 than in the non-tesseral trabecular mineralization pattern. By extension of the body zone

414 correlation with trabecular mineralization, we propose that trabecular mineralization of some
415 fossil elasmobranchs and holocephalans like *Palaeobates polaris* and *Cladoselache* derives
416 solely from body zones (Fig. 3G,H; Frey et al., 2019; Ørvig, 1951). Given such dramatic variation
417 in extant and fossil chondrichthyans, cellular and molecular mechanisms underlying the
418 evolution of tesseral and non-tesseral mineralization patterns is a wide open field of future
419 study.

420 Finally, three independent features of the adult ratfish endoskeleton argued that
421 chimaeras might have paedomorphic skeletal development, compared to elasmobranchs. First,
422 tissue mineral density (TMD) was significantly lower in a number of adult ratfish skeletal
423 elements, compared to adult little skate and catshark. Reduced TMD might reflect
424 paedomorphism, because as mineralized skeletal tissues develop, their TMD tends to increase
425 (Forbes, 1976). Indeed, the TMD of adult ratfish centra was comparable to the TMD of
426 embryonic little skate centra. Second, the morphology of adult ratfish mineralized centra was
427 comparable to the morphology of embryonic little skate mineralized centra. Mineralized centra
428 in chimaeras were thought to be unconstricted (Didier, 1995; Gadow and Abbott, 1895), but
429 micro-CT renderings of ratfish centra showed slight constriction, which was like those of centra
430 in little skate embryos. Finally, even histological similarities of centra in little skate embryos and
431 adult ratfish were discovered, since both had elongate cell lacunae organized in concentric
432 lamellae only in the mineralized middle layer of the centrum. These findings independently
433 supported a previous assertion that the perichordal sheath in adult chimaeras remained at a
434 stage corresponding to that of embryonic elasmobranchs (Gadow and Abbott, 1895), but also
435 extend it to apply to chimaera skeletal development generally.

436 Reduced skeletal mineralization in chimaeras should be investigated further, especially
437 since the only published full chondrichthyan genome was from *Callorhinchus milii*
438 (Callorhinchidae) (Venkatesh et al., 2014), and compared to other chimaera families,
439 callorhinchidaes appear to demonstrate less skeletal mineralization. For example,
440 callorhinchidaes are the only chimaera family that do not mineralize their centra (Fig. 7; Didier,
441 1995; Gadow and Abbott, 1895). The genetic basis of skeletal mineralization in vertebrates is
442 linked to the secretory calcium-binding phosphoprotein (SCPP) family of genes (Kawasaki et al.,
443 2004; Kawasaki and Weiss, 2003), none of which is present in the genome of *Callorhinchus milii*
444 (Venkatesh et al., 2014). Elasmobranch data are sparse, but catshark ameloblasts express an
445 *SCPP* gene (Leurs et al., 2022). Like elasmobranchs, the basal ray-fin fish order Acipenseriformes
446 (sturgeons, paddlefish) also have a predominantly cartilaginous skeleton, bone-like tissues, and
447 *SCPP* genes (Cheng et al., 2021; Leprevost et al., 2017; Mikami et al., 2022; Warth et al., 2017).
448 Future studies should carefully assess the potential role of *SCPP* genes in the mineralization of
449 diverse chondrichthyan mineralized tissue types.
450

451 ## Materials and Methods

452 **Specimens**

453 All samples were approved for use under the University of Saskatchewan ethical
454 protocol (AUP 20130092). Vertebrae from three samples of adult small-spotted catshark with
455 total lengths of 31 cm were provided by the University of Montpellier Aquarium (Planet Ocean
456 Montpellier). Adult, juvenile, and embryonic samples of the little skate were obtained from
457 Marine Biological Labs (Falmouth, MA, USA). Four samples of adult little skate with total lengths

458 (TL) ranging from 43.5 cm – 47.5 cm were sampled (SupTable 1). Little skate juveniles (n=7)
459 were staged by measuring their TL and disc widths (DW) and ranged from 5.5 cm DW, 10 cm TL
460 to 6.5 cm DW, 11 cm TL (SupTable 1; Stehmann, 2002). The average DW and TL of stage 32
461 embryos (n=6) and stage 33 embryos (n=6) were 3.2 cm DW, 7.5 cm TL and 3.5 cm DW, 8 cm TL,
462 respectively (SupTable 1; Maxwell et al., 2008; Vazquez et al., 2020). Five samples of adult
463 spotted ratfish with total lengths ranging from 28.5 cm to 45 cm were captured by deep-water
464 trawl in the San Juan Islands, WA (SupTable 1).

465 Regions of interest, such as ceratohyal, synarcual, and precaudal and caudal vertebrae,
466 were dissected from the little skate, catshark, and ratfish samples (SupTable 1). Dissected
467 tissues were preserved by fixation in 4% paraformaldehyde in PBS (pH 7.4) and dehydrated
468 through a graded ethanol series. Tissues for section histology were not demineralized before
469 sectioning. Tissues were embedded in optimum cutting temperature compound (Tissue Tek,
470 Torrance, CA, United States), and serial tissue sections of 10 µm thickness were made with a
471 Cryostar NX50 cryostat (Fisher Scientific, United States).

472

473 **Micro-CT imaging and data processing**

474 Desktop micro-CT imaging of little skate and ratfish tissues was done using SkyScan 1172
475 desktop microtomograph (Bruker SkyScan, Kontich, Belgium). Desktop micro-CT projections
476 were acquired using a 0.5 mm aluminium filter at 40 kV and 250 µA, 100 ms exposure time, and
477 10 µm voxel resolution, and reconstructed using NRecon (Bruker SkyScan, Kontich, Belgium). An
478 anterior region of the ratfish was cut into parts before scanning (Fig. 1A). Scans from the
479 different parts were later stitched together using Dragonfly v2021.1 (Object Research Systems,

480 Canada). Desktop imaging of catshark samples was performed as previously described (Berio et
481 al., 2021). Tissue mineral density (TMD) was quantitated on desktop micro-CT images using
482 CTAnalyzer v1.16 (CTAn, Bruker SkyScan, Kontich, Belgium) as previously described (Atake et al.,
483 2019).

484 Synchrotron radiation (SR)-based micro-CT imaging was done on the Biomedical Imaging
485 and Therapy-Insertion Device 05ID-2 (BMIT-ID) line at the Canadian Light Source. SR micro-CT
486 projections were acquired with a 28 keV photon energy, 1.44 µm voxel resolution, 1s exposure
487 time, and a sample to detector distance of 9 cm. Reconstruction of SR micro-CT projections and
488 phase retrieval was done using UFO-KIT software (https://github.com/ufo-kit/ufo-core.git). A
489 delta/beta ratio of 200 was applied during phase retrieval. 3D rendered volumes and 2D virtual
490 slices of reconstructed data were generated with Amira 6.0 (FEI Group, USA). 3D segmentation
491 and color-coding of morphological features were done using segmentation editor tools in
492 Amira.

493

494 **Histological and immunofluorescence assays**

495 Tissue sections were stained as described with Safranin O (Ferguson et al., 1998),
496 picrosirius red (Junqueira et al., 1978), or Milligan's Trichrome (Ashique et al., 2022). Alcian
497 blue/Alizarin red staining was done using a modified acid-free protocol (Eames et al., 2011).
498 Briefly, tissues sections were washed with 100 mM Tris pH 7.5/10 mM $MgCl_2$, stained with
499 0.04% Alcian blue/70%EtOH/10mM $MgCl_2$ pH 7.5, taken through graded EtOH series (80%
500 EtOH/100 mM Tris pH 7.5/10 mM MgCl2; 50% EtOH/100 mM Tris pH 7.5; 25% EtOH/100 mM
501 Tris pH 7.5), stained with 0.1% Alizarin red/0.1 % KOH pH 7.5, de-stained with two washes of

502 0.1% KOH, and dehydrated through 25% EtOH, 50% EtOH, 80% EtOH, and 100% EtOH series
503 before coverslipping. Tissue sections were demineralized using 5% EDTA for 10 mins before
504 staining with Safranin O to improve staining of mineralized cartilage.

505 To minimize the chances of tissues falling off slides, tissue sections for
506 immunofluorescence were incubated at 55°C for 15 mins before treatments and then washed
507 with PBST (1xPBS/0.5x triton-X) between subsequent treatments. Tissues were treated
508 separately with trypsin (0.1% in 5%EDTA/1xPBS) and hyaluronidase (0.5% in 1xPBS/0.5x triton-
509 X) at 37°C for 15 mins each. The tissues were blocked with 4% goat serum/2% sheep/1xPBS for
510 1 hr, and labelled with Col2 antibody (1:100, II-II6B3, Hybridoma Bank) overnight at 4°C.
511 Secondary antibody labelling was done using 488-conjugated goat anti-mouse antibody
512 (1:1000, A32723 ThermoFisher Scientific) for 3 hours.

513

514 **Quantitative and statistical analyses**

515 Statistical analyses of TMDs were performed using SPSS V.22 (SPSS). Shapiro–Wilk test was
516 used to test for normal distribution of data. To assess differences among means, one-way
517 analysis of variance (ANOVA) was used followed by Tukey HSD or Games-Howell post hoc
518 analyses, depending upon whether homogeneity of variance assumption was met or not,
519 respectively.

520

521 **Data availability**

522 Raw data from microCT projections and quantitative measurements have been deposited at
523 Dryad (DOI: 10.5061/dryad.crjdfn3b9) and can be accessed at
524 https://datadryad.org/stash/share/gnKH8kfRoKdHRE9rFGDausGzBZ1VTuCK3DB5gRPkrnp
525

526 **Acknowledgements**

527 This work was funded by Natural Sciences and Engineering Research Council (NSERC) grants
528 RGPIN 435655-201 and RGPIN 2014-05563 awarded to BFE. The authors are very thankful to
529 Adam Summers of Friday Harbor in the San Juan Islands for providing the spotted ratfish
530 samples and some feedback on the spotted ratfish data. Research described in this paper was
531 performed at the BMIT facility at the Canadian Light Source, which is supported by Canada
532 Foundation for Innovation, Natural Sciences and Engineering Research Council of Canada, the
533 University of Saskatchewan, Western Economic Diversification Canada, the National Research
534 Council Canada, and the Canadian Institutes of Health Research. We acknowledge the MRI
535 platform member of the national infrastructure France-BioImaging supported by the French
536 National Research Agency (ANR-10-INBS- 04, "Investments for the future"), the labex CEMEB
537 (ANR-10-LABX-0004) and NUMEV (ANR-10-LABX-0020).
538

539 **Figure legends**

540 Figure 1. Mineralized tissues were abundant in the spotted ratfish, but they had lower tissue
541 mineral density (TMD) compared to the little skate and the small-spotted catshark. (**A**)
542 Photograph of the ratfish *Hydrolagus colliei* illustrating the anterior region that was micro-CT
543 imaged. (**B-G**) Micro-CT 3D renderings of the anterior region of ratfish (B) showed mineralized
544 tissues in neural arches, basidorsals, and centra in segmented vertebrae (C,D), in the ceratohyal
545 and other skeletal elements in the pharyngeal skeleton (E), and in the fused vertebral synarcual
546 (F,G). (**H**) Comparative quantitative analyses showed that TMD of the synarcual, neural arch,
547 and centra in ratfish were significantly lower than TMDs of same regions in little skate and
548 catshark. Abbreviations: A, anterior; bb, basibranchial; bd, basidorsal; bh, basihyal; c, centrum
549 cb, ceratobranchial; ch, ceratohyal; D, dorsal; hbs, hypobranchials; L, left; MK, Meckel's; na,
550 neural arch; P, posterior; R, right; snf, spinal nerve foramina; V, ventral. * indicates statistically
551 significant comparison (p<0.05). Scale bars: as indicated.

552

553 Figure 2. Ratfish lack neural arch bone-like tissue. (**A-C**) Micro-CT 3D renderings showed a
554 compact mineralization pattern of bone-like tissue in neural arches of segmented vertebrae in
555 little skate (A) and catshark (B), and an irregular pattern of mineralized tissues in ratfish (C). (**D-**
556 **F**) Micro-CT 2D virtual slices showing that the bone-like tissue in little skate and catshark was
557 extensively mineralized and surrounded a neural arch core (D,E), whereas irregular mineralized
558 tissues in ratfish neural arches were restricted to medial and lateral periphery (F). (**G-L**) Section
559 histology showed Alizarin red staining of continuous mineralization and birefringent collagen
560 fibers in neural arch bone-like tissues in little skate (G,J) and catshark (H,K), but not in ratfish

561 (I,L). Picrosirius red staining also revealed some birefringent fibers (likely reticular) in muscles
562 on the lateral sides of neural arches in little skate, catshark, and ratfish (J-L). Irregular
563 mineralized tissue in the ratfish neural arch was discretely organized, Alizarin red-positive, and
564 Col2-positive mineralized cartilage (I,L). Other regions of ratfish were Alcian blue-positive and
565 Col2-positive unmineralized cartilage (I,L). The neural arch core in little skate and catshark
566 consisted of mineralized cartilage (MC) and mostly unmineralized cartilage, respectively (J,K).
567 Abbreviations: 2D, two-dimensional; 3D, three-dimensional; Ab, Alcian blue; Ar, Alizarin red;
568 BLT, bone-like tissue; c, cartilage; Col2, collagen type 2; D, dorsal; IF, immunofluorescence; L,
569 lateral; M, medial; MC, mineralized cartilage; PSR, picrosirius red; V, ventral. Scale bars: as
570 indicated.
571
572 Figure 3. Little skate, catshark, and ratfish all showed trabecular mineralization but without the
573 bone-like cap zone in catshark and ratfish. (**A-D**) Micro-CT renderings of the little skate
574 hyomandibula and precaudal vertebra (A,B), catshark caudal vertebra (C), and ratfish ceratohyal
575 (D). (**E-H**) Tesseral and non-tesseral mineralization patterns in little skate, catshark, and ratfish.
576 The little skate hyomandibula displayed a superficial polygonal tesseral pattern (E') and an
577 underlying trabecular tesseral pattern (E"), while regions of the little skate neural spine only
578 displayed a trabecular tesseral pattern (F). The catshark haemal arch (G), and ratfish ceratohyal
579 (H) displayed a non-tesseral trabecular pattern. Regions for hi-mag views in panels E'-H are
580 indicated in corresponding panels of A-D. (**I-T**) Histological and immunofluorescent features of
581 tesseral or non-tesseral mineralized tissues in little skate (I,J,M,N,Q,R), catshark (K,O,S), and
582 ratfish (L,P,T). Alizarin red staining, Safranin O staining, and Col2 immunofluorescence showed

583 that little skate, catshark, and ratfish had the body zone of mineralized cartilage (I-T). The bone-
584 like tesseral cap zone consisting of elongate lacunae in matrix that is mineralized (I,J), Safranin
585 O-negative (M,N), Col2-negative (Q,R), and contains birefringent collagen fibers (Q,R) was
586 present only in polygonal tesserae and trabecular tesserae in little skate. Abbreviations: Ab,
587 Alcian blue; Ar, Alizarin red; Bz, body zone; c, cartilage; Col2, collagen type 2; Cz, cap zone; D,
588 dorsal; IF, immunofluorescence; L, lateral; M, medial; PSR, picrosirius red; NA, neural arch; NS,
589 neural spine; V, ventral. Scale bars: as indicated.
590
591 Figure 4. Micro-CT segmentation clearly correlated histological features of mineralized tissues
592 with their mineralization patterns . (**A-J**) Trichrome's acid fucshin marked the larger and smaller
593 cap zones of little skate polygonal and trabecular tesserae, respectively (A,F). 3D renderings of
594 polygonal tesserae showed that the cap zone (Cz, segmented in red) was superficial and
595 reflected the polygonal pattern (B-D). The smaller cap zone in trabecular tesserae was not
596 laterally extensive enough to display a superficial polygonal pattern like that of polygonal
597 tesserae (B-D,G-I). Spokes in polygonal and trabecular tesserae did not stain with Trichrome (*
598 in A,F). 3D renderings showed that spokes (*, segmented in blue) in the deeper body zones
599 displayed a radiating pattern like the trabecular patterns in little skate polygonal and trabecular
600 tesserae (A-C,E,F-J). (**K-O**) Trichrome staining demonstrated that trabecular mineralized tissue
601 in ratfish lacked a cap zone but had other features, such as a body zone and intertesseral fibres
602 (K). Segmentation demonstrated that spokes in ratfish were patchy and did not display a
603 radiating trabecular pattern (K-O). Abbreviations: Bz, body zone; Cz, cap zone; ITF, intertesseral
604 fibres. Scale bars: as indicated.

605

606 Figure 5. Ratfish centra had the same features as areolar mineralized tissues in little skate and
607 catshark. (**A-C**) Micro-CT renderings demonstrated that centra in little skate and catshark had a
608 compact mineralization and a gross biconcave morphology (A,B), while centra in ratfish also
609 displayed a compact mineralization pattern but were organized in multiple rings (C). (**D-O**)
610 Consistent with areolar mineralized tissue in little skate (D,G) and catshark (E,H), Alcian
611 blue/Alizarin section histology (Ab/Ar) showed that mineralized centra in ratfish consisted of a
612 mineralized areolar centra layer with elongate lacunae in concentric lamellae (F,I). Regions for
613 hi-mag views in panels G-O are indicated in corresponding panels of D-F; regions for hi-mag
614 inserts in panels G-I are indicated in those panels. Areolar mineralized tissue in little skate
615 lacked Safranin O staining and Col2 immunofluorescence (J,M), while catshark areolar
616 mineralized tissue demonstrated weak Safranin O staining and Col2 immunofluorescence (K,N).
617 Safranin O staining and Col2 immunofluorescence highlighted cartilaginous matrix of areolar
618 mineralized tissue in ratfish (L,O). Little skate also had mineralization in both outer and inner
619 centra layers (G), while catshark also had an outer mineralized layer (H), and these additional
620 centra layers demonstrated weak Safranin O staining and Col2 immunofluorescence (J,M,K,N).
621 Abbreviations: A, anterior; Ab, Alcian blue; Ar, Alizarin red; c, cartilage; Col2, collagen type 2; D,
622 dorsal; IF, immunofluorescence; IL, inner layer; L, lateral; M, medial, OL, outer layer; P,
623 posterior; V, ventral. Scale bars: as indicated; inserts in G-I are 20 µm.

624

625 Figure 6. Morphological and histological features of centra in little skate embryos and juveniles
626 suggested that the adult ratfish demonstrated paedomorphic centra. (**A-D**) Desktop micro-CT

627 renderings showed centrum and other mineralized structures in vertebral segments (dashed
628 lines) of little skate embryos and juveniles (A-C) and adult ratfish (D). (**E-H**) Synchrotron
629 radiation micro-CT renderings of centra in little skate embryos and juveniles (E-G) and adult
630 ratfish (H) showed that centra in the ratfish were slightly constricted like those of little skate
631 embryos (red arrows). (**I-K**) Alcian blue/Alizarin red section histology showed that areolar
632 mineralized tissue constituted the only centra layer in little skate embryos (I,J), whereas an
633 outer mineralized centra layer was present in 6.5 cm DW juveniles (K). (**L**) Tissue mineral
634 density (TMD) of centra in ratfish was similar to those of stage 33 embryos and 6.5 cm DW
635 juveniles of little skate. Abbreviation: A, anterior; Ab, Alcian blue; Ar, Alizarin red; bd,
636 basidorsal; C, centrum; HA, haemal arch; L, lateral; M, medial; NA, neural arch; OL, outer layer;
637 P, posterior.* indicates statistically significant comparison (p<0.05). Scale bars: as indicated.
638
639 Figure 7. Character states of mineralized tissues in various chondrichthyan clades suggest
640 shared and derived features. The absence of neural arch bone-like tissue (BLT) in holocephalans
641 and ancestral crown chondrichthyans (from fossils) would further support the conclusion that
642 neural arch bone-like tissue is a synapomorphic (shared derived) character of elasmobranchs.
643 Polygonal (PT) and trabecular (TT) tesseral mineralization patterns appear to be absent in
644 extant holocephalans and stem chondrichthyans, but their presence in some elasmobranchs
645 and some fossil holocephalans suggest that these tesseral mineralizations are synapomorphic
646 characters of crown chondrichthyans. Non-tesseral trabecular mineralization (NTT) is a
647 symplesiomorphic (shared ancestral) character of stem and crown chondrichthyans, because it
648 is pervasive in ancestral and extant chondrichthyans. The histological cap zone in some

elasmobranchs, along with the inference that polygonal tesserae in fossil holocephalans means that they had cap zones, suggests that the cap zone is also a synapomorphic character of crown chondrichthyans. The presence of a histological body zone in either tesseral or non-tesseral mineralized tissues of stem and crown chondrichthyans suggests that the body zone is a symplesiomorphic character of all chondrichthyans. Areolar mineralized tissue is present in elasmobranchs and holocephalans, but its absence in stem chondrichthyans suggests that it is a synapomorphic character of crown chondrichthyans.

References

Ashique, A.M., Atake, O.J., Ovens, K., Guo, R., Pratt, I.V., Detrich III, H.W., Cooper, D.M., Desvignes, T., Postlethwait, J.H., Eames, B.F., 2022. Bone microstructure and bone mineral density are not systemically different in Antarctic icefishes and related Antarctic notothenioids. Journal of Anatomy 240, 34-49 DOI: https://doi.org/10.1111/joa.13537.

Atake, O.J., Cooper, D.M.L., Eames, B.F., 2019. Bone-like features in skate suggest a novel elasmobranch synapomorphy and deep homology of trabecular mineralization patterns. Acta Biomater 84, 424-436 DOI: 10.1016/j.actbio.2018.11.047.

Atake, O.J., Eames, B.F., 2021. Mineralized Cartilage and Bone-Like Tissues in Chondrichthyans Offer Potential Insights Into the Evolution and Development of Mineralized Tissues in the Vertebrate Endoskeleton. Frontiers in Genetics 12 DOI: 10.3389/fgene.2021.762042.

Berio, F., Broyon, M., Enault, S., Pirot, N., López-Romero, F.A., Debiais-Thibaud, M., 2021. Diversity and Evolution of Mineralized Skeletal Tissues in Chondrichthyans. Frontiers in Ecology and Evolution 9, 223 DOI: 10.3389/fevo.2021.660767.

Bordat, C., 1987. Étude ultrastructurale de l'os des vertèbres du Sélacien Scyliorhinus canicula L. Canadian Journal of Zoology 65, 1435-1444 DOI: 10.1139/z87-226.

Cheng, P., Huang, Y., Lv, Y., Du, H., Ruan, Z., Li, C., Ye, H., Zhang, H., Wu, J., Wang, C., Ruan, R., Li, Y., Bian, C., You, X., Shi, C., Han, K., Xu, J., Shi, Q., Wei, Q., 2021. The American Paddlefish Genome Provides Novel Insights into Chromosomal Evolution and Bone Mineralization in Early Vertebrates. Mol Biol Evol 38, 1595-1607 DOI: 10.1093/molbev/msaa326.

Claeson, K.M., 2011. The synarcual cartilage of batoids with emphasis on the synarcual of Rajidae. J Morphol 272, 1444-1463 DOI: 10.1002/jmor.10996.

Clement, J., 1992. Re-examination of the fine structure of endoskeletal mineralization in chondrichthyans: implications for growth, ageing and calcium homeostasis. Marine and Freshwater Research 43, 157-181.

683 Coates, M.I., Finarelli, J.A., Sansom, I.J., Andreev, P.S., Criswell, K.E., Tietjen, K., Rivers, M.L., La Riviere,
684 P.J., 2018. An early chondrichthyan and the evolutionary assembly of a shark body plan. Proc Biol Sci
685 285, 20172418 DOI: 10.1098/rspb.2017.2418.

686 Criswell, K.E., Coates, M.I., Gillis, J.A., 2017. Embryonic development of the axial column in the little
687 skate, *Leucoraja erinacea*. J Morphol 278, 300-320 DOI: 10.1002/jmor.20637.

688 Criswell, K.E., Gillis, J.A., 2020. Resegmentation is an ancestral feature of the gnathostome vertebral
689 skeleton. Elife 9, e51696 DOI: 10.7554/eLife.51696.

690 Dean, M.N., Bizzarro, J.J., Clark, B., Underwood, C.J., Johanson, Z., 2017. Large batoid fishes frequently
691 consume stingrays despite skeletal damage. Royal Society Open Science 4, 170674 DOI:
692 doi:10.1098/rsos.170674.

693 Dean, M.N., Summers, A.P., 2006. Mineralized cartilage in the skeleton of chondrichthyan fishes.
694 Zoology (Jena) 109, 164-168 DOI: 10.1016/j.zool.2006.03.002.

695 Debiais-Thibaud, M., 2018. The Evolution of Endoskeletal Mineralisation in Chondrichthyan Fish,
696 Evolution and development of fishes. Cambridge University Press, pp. 110-125.

697 Didier, D.A., 1995. Phylogenetic systematics of extant chimaeroid fishes (Holocephali, Chimaeroidei).
698 American Museum of Natural History, New York.

699 Eames, B.F., Allen, N., Young, J., Kaplan, A., Helms, J.A., Schneider, R.A., 2007. Skeletogenesis in the swell
700 shark *Cephaloscyllium ventriosum*. J Anat 210, 542-554 DOI: 10.1111/j.1469-7580.2007.00723.x.

701 Eames, B.F., Yan, Y.-L., Swartz, M.E., Levic, D.S., Knapik, E.W., Postlethwait, J.H., Kimmel, C.B., 2011.
702 Mutations in fam20b and xylt1 reveal that cartilage matrix controls timing of endochondral ossification
703 by inhibiting chondrocyte maturation. PLoS Genetics 7, e1002246 DOI: 10.1371/journal.pgen.1002246.

704 Enault, S., Munoz, D.N., Silva, W.T., Borday-Birraux, V., Bonade, M., Oulion, S., Venteo, S., Marcellini, S.,
705 Debiais-Thibaud, M., 2015. Molecular footprinting of skeletal tissues in the catshark *Scyliorhinus*
706 *canicula* and the clawed frog *Xenopus tropicalis* identifies conserved and derived features of vertebrate
707 calcification. Front Genet 6, 283 DOI: 10.3389/fgene.2015.00283.

708 Ferguson, C.M., Miclau, T., Hu, D., Alpern, E., Helms, J.A., 1998. Common molecular pathways in skeletal
709 morphogenesis and repair. Ann N Y Acad Sci 857, 33-42 DOI: 10.1111/j.1749-6632.1998.tb10105.x.

710 Forbes, G.B., 1976. Calcium accumulation by the human fetus. Pediatrics 57, 976-977 DOI:
711 10.1542/peds.57.6.976.

712 Frey, L., Coates, M., Ginter, M., Hairapetian, V., Rucklin, M., Jerjen, I., Klug, C., 2019. The early
713 elasmobranch *Phoebodus*: phylogenetic relationships, ecomorphology and a new time-scale for shark
714 evolution. Proc Biol Sci 286, 20191336 DOI: 10.1098/rspb.2019.1336.

715 Gadow, H.F., Abbott, E., 1895. IV. On the evolution of the vertebral column of fishes. Philosophical
716 Transactions of the Royal Society of London. (B.) 186, 163-221 DOI: 10.1098/rstb.1895.0004.

717 Garstang, W., 1922. The Theory of Recapitulation: A Critical Re-statement of the Biogenetic Law.
718 Zoological Journal of the Linnean Society 35, 81-101 DOI: 10.1111/j.1096-3642.1922.tb00464.x.

719 Gillis, J.A., Rawlinson, K.A., Bell, J., Lyon, W.S., Baker, C.V., Shubin, N.H., 2011. Holocephalan embryos
720 provide evidence for gill arch appendage reduction and opercular evolution in cartilaginous fishes. Proc
721 Natl Acad Sci U S A 108, 1507-1512 DOI: 10.1073/pnas.1012968108.

722 Goldring, M.B., Tsuchimochi, K., Ijiri, K., 2006. The control of chondrogenesis. J Cell Biochem 97, 33-44
723 DOI: 10.1002/jcb.20652.

724 Golub, E.E., 2009. Role of matrix vesicles in biomineralization. Biochim Biophys Acta 1790, 1592-1598
725 DOI: 10.1016/j.bbagen.2009.09.006.

726 Herbert, A.M., Dean, M.N., Summers, A.P., Wilga, C.D., 2022. Biomechanics of the jaws of spotted
727 ratfish. Journal of Experimental Biology 225 DOI: 10.1242/jeb.243748.

728 Janvier, P., 1996. Early vertebrates. Oxford University Press.

729 Jayasankar, A.K., Seidel, R., Hosny, A., Weaver, J.C., Fratzl, P., Chen, J., Dean, M.N., 2020. Multi-scale
730 modeling and mechanical performance characterization of stingray skeleton-inspired tessellations.
731 Journal of the Mechanics and Physics of Solids 138, 103906 DOI: 10.1016/j.jmps.2020.103906.

732 Johanson, Z., Boisvert, C., Maksimenko, A., Currie, P., Trinajstic, K., 2015. Development of the Synarcual
733 in the Elephant Sharks (Holocephali; Chondrichthyes): Implications for Vertebral Formation and Fusion.
734 PLoS One 10, e0135138 DOI: 10.1371/journal.pone.0135138.

735 Johanson, Z., Trinajstic, K., Carr, R., Ritchie, A., 2012. Evolution and development of the synarcual in
736 early vertebrates. Zoomorphology 132, 95-110 DOI: 10.1007/s00435-012-0169-9.

737 Junqueira, L.C., Cossermelli, W., Brentani, R., 1978. Differential staining of collagens type I, II and III by
738 Sirius Red and polarization microscopy. Arch Histol Jpn 41, 267-274 DOI: 10.1679/aohc1950.41.267.

739 Kawasaki, K., Suzuki, T., Weiss, K.M., 2004. Genetic basis for the evolution of vertebrate mineralized
740 tissue. Proceedings of the National Academy of Sciences 101, 11356-11361 DOI:
741 doi:10.1073/pnas.0404279101.

742 Kawasaki, K., Weiss, K.M., 2003. Mineralized tissue and vertebrate evolution: The secretory calcium-
743 binding phosphoprotein gene cluster. Proceedings of the National Academy of Sciences 100, 4060-4065
744 DOI: doi:10.1073/pnas.0638023100.

745 Kemp, N.E., Westrin, S.K., 1979. Ultrastructure of calcified cartilage in the endoskeletal tesserae of
746 sharks. J Morphol 160, 75-109 DOI: 10.1002/jmor.1051600106.

747 Leprevost, A., Azals, T., Trichet, M., Sire, J.Y., 2017. Vertebral Development and Ossification in the
748 Siberian Sturgeon (Acipenser Baerii), with New Insights on Bone Histology and Ultrastructure of
749 Vertebral Elements and Scutes. Anat Rec (Hoboken) 300, 437-449 DOI: 10.1002/ar.23515.

750 Leurs, N., Martinand-Mari, C., Marcellini, S., Debiais-Thibaud, M., 2022. Parallel Evolution of
751 Ameloblastic scpp Genes in Bony and Cartilaginous Vertebrates. Molecular Biology and Evolution 39
752 DOI: 10.1093/molbev/msac099.

753 Lowenstam, H.A., 1981. Minerals formed by organisms. Science 211, 1126-1131 DOI:
754 10.1126/science.7008198.

755 Maisey, J.G., 2013. The diversity of tessellated calcification in modern and extinct chondrichthyans.
756 Revue de Paléobiologie 32, 355-371.

Maisey, J.G., Denton, J.S.S., Burrow, C., Pradel, A., 2021. Architectural and ultrastructural features of tessellated calcified cartilage in modern and extinct chondrichthyan fishes. J Fish Biol 98, 919-941 DOI: 10.1111/jfb.14376.

Marrama, G., Schultz, O., Kriwet, J., 2019. A new Miocene skate from the Central Paratethys (Upper Austria): the first unambiguous skeletal record for the Rajiformes (Chondrichthyes: Batomorphii). J Syst Palaeontol 17, 937-960 DOI: 10.1080/14772019.2018.1486336.

Maxwell, E.E., Fröbisch, N.B., Heppleston, A.C., 2008. Variability and Conservation in Late Chondrichthyan Development: Ontogeny of the Winter Skate (Leucoraja ocellata). The Anatomical Record 291, 1079-1087 DOI: https://doi.org/10.1002/ar.20719.

Mikami, M., Ineno, T., Thompson, A.W., Braasch, I., Ishiyama, M., Kawasaki, K., 2022. Convergent losses of SCPP genes and ganoid scales among non-teleost actinopterygians. Gene 811, 146091 DOI: https://doi.org/10.1016/j.gene.2021.146091.

Miles, R.S., 1970. Remarks on the Vertebral Column and Caudal Fin of Acanthodian Fishes. Lethaia 3, 343-362 DOI: 10.1111/j.1502-3931.1970.tb00828.x.

Omelon, S., Georgiou, J., Variola, F., Dean, M.N., 2014. Colocation and role of polyphosphates and alkaline phosphatase in apatite biomineralization of elasmobranch tesserae. Acta Biomater 10, 3899-3910 DOI: 10.1016/j.actbio.2014.06.008.

Ørvig, T., 1951. The endoskeleton, with remarks on the hard tissues of lower vertebrates in general, Histologic studies of Placoderms and fossil Elasmobranchs. Almqvist & Wiksell, Stockholm, pp. 321-454.

Pears, J.B., Johanson, Z., Trinajstic, K., Dean, M.N., Boisvert, C.A., 2020. Mineralization of the *Callorhinchus* Vertebral Column (Holocephali; Chondrichthyes). Front Genet 11, 571694 DOI: 10.3389/fgene.2020.571694.

Peignoux-Deville, J., Lallier, F., Vidal, B., 1982. Evidence for the presence of osseous tissue in dogfish vertebrae. Cell Tissue Res 222, 605-614 DOI: 10.1007/BF00213858.

Porter, M.E., Beltrán, J.L., Koob, T.J., Summers, A.P., 2006. Material properties and biochemical composition of mineralized vertebral cartilage in seven elasmobranch species (Chondrichthyes). J Exp Biol 209, 2920-2928 DOI: 10.1242/jeb.02325.

Ridewood, W., MacBride, E.W., 1921. VIII.—On the calcification of the vertebral centra in sharks and rays. Philosophical Transactions of the Royal Society of London. Series B, Containing Papers of a Biological Character 210, 311-407 DOI: 10.1098/rstb.1921.0008.

Rossert, J., de Crombrugghe, B., 2002. Type I collagen: structure, synthesis, and regulation, Principles of bone biology. Elsevier, pp. 189-XVIII.

Seidel, R., Blumer, M., Chaumel, J., Amini, S., Dean, M.N., 2020. Endoskeletal mineralization in chimaera and a comparative guide to tessellated cartilage in chondrichthyan fishes (sharks, rays and chimaera). J R Soc Interface 17, 20200474 DOI: 10.1098/rsif.2020.0474.

Seidel, R., Blumer, M., Pechriggl, E.J., Lyons, K., Hall, B.K., Fratzl, P., Weaver, J.C., Dean, M.N., 2017. Calcified cartilage or bone? Collagens in the tessellated endoskeletons of cartilaginous fish (sharks and rays). J Struct Biol 200, 54-71 DOI: 10.1016/j.jsb.2017.09.005.

Seidel, R., Lyons, K., Blumer, M., Zaslansky, P., Fratzl, P., Weaver, J.C., Dean, M.N., 2016. Ultrastructural and developmental features of the tessellated endoskeleton of elasmobranchs (sharks and rays). J Anat 229, 681-702 DOI: 10.1111/joa.12508.

Smith, M., Manzanares, E., Underwood, C., Healy, C., Clark, B., Johanson, Z., 2020. Holocephalan (Chondrichthyes) dental plates with hypermineralized dentine as a substitute for missing teeth through developmental plasticity. J Fish Biol 97, 16-27 DOI: 10.1111/jfb.14302.

Smith, M.M., Hall, B.K., 1990. Development and evolutionary origins of vertebrate skeletogenic and odontogenic tissues. Biol Rev Camb Philos Soc 65, 277-373 DOI: 10.1111/j.1469-185x.1990.tb01427.x.

Stehmann, M.F., 2002. Proposal of a maturity stages scale for oviparous and viviparous cartilaginous fishes (Pisces, Chondrichthyes). Archive of Fishery and Marine research 50, 23-48.

Vazquez, D.M., Díaz de Astarloa, J.M., Gabbanelli, V., Mabragaña, E., 2020. Comparative embryonic development patterns in three deep-water skates from the southwest Atlantic. Deep Sea Research Part I: Oceanographic Research Papers 161, 103301 DOI: 10.1016/j.dsr.2020.103301.

Venkatesh, B., Lee, A.P., Ravi, V., Maurya, A.K., Lian, M.M., Swann, J.B., Ohta, Y., Flajnik, M.F., Sutoh, Y., Kasahara, M., Hoon, S., Gangu, V., Roy, S.W., Irimia, M., Korzh, V., Kondrychyn, I., Lim, Z.W., Tay, B.-H., Tohari, S., Kong, K.W., Ho, S., Lorente-Galdos, B., Quilez, J., Marques-Bonet, T., Raney, B.J., Ingham,

811 P.W., Tay, A., Hillier, L.W., Minx, P., Boehm, T., Wilson, R.K., Brenner, S., Warren, W.C., 2014. Elephant
812 shark genome provides unique insights into gnathostome evolution. Nature 505, 174-179 DOI:
813 10.1038/nature12826.

814 Warth, P., Hilton, E.J., Naumann, B., Olsson, L., Konstantinidis, P., 2017. Development of the skull and
815 pectoral girdle in Siberian sturgeon, *Acipenser baerii*, and Russian sturgeon, *Acipenser gueldenstaedtii*
816 (Acipenseriformes: Acipenseridae). J Morphol 278, 418-442 DOI: 10.1002/jmor.20653.

817 Wilga, C.A.D., Ferry, L.A., 2015. 4 - Functional Anatomy and Biomechanics of Feeding in Elasmobranchs,
818 in: Shadwick, R.E., Farrell, A.P., Brauner, C.J. (Eds.), Fish Physiology. Academic Press, pp. 153-187.

819